The effect of intermolecular interactions on the electric properties of helium and argon. III. Quantum statistical calculations of the dielectric second virial coefficients

Antonio Rizzo[a)]
Istituto per i Processi Chimico-Fisici del Consiglio Nazionale delle Ricerche, Area della Ricerca, via G. Moruzzi 1, loc. S. Cataldo, I-56124 Pisa, Italy

Christof Hättig
Forschungszentrum Karlsruhe, Institute of Nanotechnology, P.O. Box 3640, D-76021 Karlsruhe, Germany

Berta Fernández and Henrik Koch[b)]
Department of Physical Chemistry, Faculty of Chemistry, University of Santiago de Compostela, E-15782 Santiago de Compostela, Spain

(Received 1 April 2002; accepted 15 May 2002)

The second dielectric virial coefficients of helium and argon are investigated using a fully quantum statistical approach and recent accurate *ab initio* results for the interatomic potentials and the interaction-induced polarizabilities. We thereby extend a preceding investigation based on a semiclassical approach to include quantum effects. For helium the results support the findings of a previous study by Moszynski *et al.* [J. Chem. Phys. **247**, 440 (1995)] that quantum effects are substantial for temperatures below 10 K, while they are practically negligible above 70 K. For argon special care is needed in the numerical integrations carried out in the quantum statistical calculation of the virial coefficients, due to the presence of quasibound states in the continuum and a slow convergence of the summation over the angular momentum. Here quantum effects are practically negligible in the range of temperatures experimentally investigated, i.e., between 243 and 408 K. As far as comparison with experimental data is concerned, large discrepancies are found for some of the low-temperature experimental measurements of helium. Agreement is also unsatisfactory for high temperatures for argon and experimental redetermination is suggested. © *2002 American Institute of Physics.* [DOI: 10.1063/1.1491402]

I. INTRODUCTION

In recent publications[1–3] we studied the second virial coefficients for some optical properties of helium and argon. Virial coefficients describe the second-order contribution to the pressure dependence of properties caused by pair interactions in the gas phase. Among the coefficients studied in Refs. 1 and 3 were the dielectric and the refractivity second virial coefficients, which describe the second-order pressure dependence of, respectively, the dielectric constant and the refractive index. Furthermore the second Kerr virial coefficient and the second virial coefficient of the electric field induced second harmonic generation (ESHG) hyperpolarizability were investigated.[1,3] One of the present authors (A.R.) was also involved in the study of other interaction-induced properties of the helium atom, i.e., the dependence on the pressure of the chemical shielding[4] and that of the magnetizability, hypermagnetizability, and the Cotton–Mouton effect.[5]

In the studies of Refs. 1, 2, and 3 we performed accurate *ab initio* calculations for the interaction-induced dipole polarizabilities, both average—$\Delta\alpha_{\mathrm{ave}}(R)$—and anisotropy—$\Delta\alpha_{\mathrm{ani}}(R)$, and isotropic second hyperpolarizabilities—$\Delta\gamma_{\|}$—using highly correlated electron structure methods and extensive basis sets. For helium both full configuration interaction (FCI) and coupled cluster singles and doubles (CCSD) calculations were carried out, using correlation consistent basis sets which are denoted as d-aug-cc-pVTZ-3321 and d-aug-cc-pV5Z-3321, respectively. The extension ''3321'' indicates the addition of a $3s3p2d1f$ set of midbond functions to the original basis sets of Dunning and co-workers. The difference between the CCSD/d-aug-cc-pV5Z-3321 and CCSD/d-aug-cc-pVTZ-3321 results was used to partially correct the FCI/d-aug-cc-pVTZ-3321 results for the residual basis set error. For argon the CCSD response approach and a d-aug-cc-pVQZ-33211 basis set were employed to compute the interaction-induced properties. From an analysis of basis set and electron correlation effects we could conclude that using a basis set larger than d-aug-cc-pVQZ-33211 and introducing correlation effects beyond CCSD yield very small effects of equal magnitude for the isotropic properties $\Delta\alpha_{\mathrm{ave}}$ and $\Delta\gamma_{\|}$, whereas higher-order correlation effects become considerably more important—although still rather small—for the potential energy and for anisotropic properties as e.g. $\Delta\alpha_{\mathrm{ani}}$. To account for the frequency dependence of the second refractivity and the second hyperpolarizability (Kerr and ESHG) virial coefficients the interaction-induced polarizabilities and hyperpolarizabilities were expanded in power series in terms of Cauchy moments and hyperpolarizability disper-

a)Electronic mail: rizzo@icqem.pi.cnr.it
b)Permanent address: Department of Chemistry, University of Southern Denmark, DK-5230 Odense M, Denmark.

 © 2002 American Institute of Physics

Downloaded 26 Jul 2002 to 141.52.232.84. Redistribution subject to AIP license or copyright, see http://ojps.aip.org/jcpo/jcpcr.jsp

sion coefficients. For most of the second virial coefficients it was found that the effect of the frequency dependence is small.

In our previous studies we employed a semiclassical approximation for the radial distribution function to calculate the second virial coefficients from the *ab initio* results for the interaction-induced properties. This approximation becomes exact in the limit of high temperatures, but it breaks down at low temperatures, due to neglect of the quantum effects. For the second dielectric virial coefficient of helium we could observe good agreement between our results and some of the experimental estimates at temperatures higher than 70 K. In the case of argon, the agreement between theoretical and experimental results is reasonable for temperatures in the range between 242 and 303 K, but unsatisfactory for higher temperatures. For both systems, some of the experimental data carry large error bars.

A detailed review of previous experimental and theoretical investigations on the helium and argon dielectric virial coefficients is given in Refs. 1 and 3. The second dielectric coefficient of argon was measured at several temperatures by different authors: Vidal and Lallemand,[6] Bose *et al.*,[7–9] Johnston *et al.*,[10] Orcutt and Cole,[11] and Proffit *et al.*[12] Previous *ab initio* calculations[7,13,14] were in disagreement with each other and with experiment. Discrepancies arose both from the neglect of electron correlation effects and from the large uncertainties of the experimental results. The dielectric virial coefficient of helium has been measured both by direct[6,11,15,16] and indirect[7,14,17–19] methods at temperatures ranging from as low as 3.799 K up to 323.15 K. At low temperatures the measured data are highly scattered.

Theoretical investigations of the helium second dielectric virial coefficient have been carried out by several groups (see Ref. 3 for details). Quantum calculations of the second dielectric virial coefficients of helium were the subject of a few studies in the 1960s and 1970s by Ishihara and co-workers,[20,21] McQuarrie and Levine,[22] Ely and McQuarrie,[23] and Bruch, Fortune, and Berman.[24] In some cases[23,24] the approach adopted was an expansion of the semiclassical expression for the dielectric virial coefficients in powers of $\hbar^2$, leading to quantum corrections to the semiclassical formula up to fourth order in $\hbar$. Estimates were thus obtained for a Lennard-Jones potential and dipole–induced-dipole interaction-induced polarizability averages,[23] and for an approximate pair distribution function together with coupled-Hartree–Fock diatomic polarizabilities.[24]

In 1995 Moszynski and co-workers[25] presented the results of a fully quantum statistical calculation of the second dielectric virial coefficient of helium based on an accurate empirical potential and symmetry-adapted perturbation theory (SAPT) results for the interaction-induced polarizability.[26,27] This study showed that quantum effects become substantial for temperatures below ≈ 10 K, while they are small for $T > 100$ K. To our knowledge, this is to date the only *ab initio* calculation exploiting a fully quantum statistical approach for a second virial coefficient. There has been no systematic investigation on the importance of quantum effects for second dielectric virial coefficients for systems other than helium. It is therefore unknown in which temperature range and for which systems quantum effects in general become significant and the semiclassical approximation breaks down.

In this paper we present an extension of a previous semiclassical investigation of the second dielectric virial coefficients of helium and argon to a fully quantum statistical treatment along the lines of Ref. 25, which are briefly summarized in Sec. II. For helium, where the dimer has a very weakly bound interatomic potential, the calculations can be carried out rather straightforwardly, using standard integration schemes. For argon, however, the presence of quasibound states in the continuum and a slow convergence of the summation over the angular momentum lead to several computational difficulties which require the adoption of special integration algorithms. The implementation of the quantum statistical approach and the integration schemes are outlined in Sec. III, where also the computational details are given. The results are presented and discussed in Sec. IV, which is followed by some concluding remarks in Sec. V.

II. THEORY

The general theory for a quantum-statistical evaluation of dielectric second virial coefficients dates back to the early years of quantum mechanics. Thus the basic ingredients for the derivation of a fully quantum statistical expression for the virial coefficients can be found in several textbooks on molecular theory of gases and liquids, see for instance Refs. 28 and 29.

The Clausius–Mossotti function in dilute atomic gases can be expanded in orders of the molar density ρ (the inverse molar volume) of the gas, and the dielectric second virial coefficient can be obtained[30] from the quadratic correction given by $B_\epsilon(T)\rho^2$. For thermal energies large compared to the dissociation energy of the dimer, the semiclassical approximation for the $B_\epsilon(T)$ holds valid and for a diatomic dimer

$$B_\epsilon(T) = \frac{N_A^2}{6\epsilon_0} 4\pi \int_0^\infty \Delta\alpha_{\mathrm{ave}}(R) e^{-V(R)/k_B T} R^2 dR, \tag{1}$$

where T is the temperature, R the internuclear distance, N_A is Avogadro's number, k_B is Boltzmann's constant, ϵ_0 the vacuum permittivity, $V(R)$ the dimer interatomic potential, and $\Delta\alpha_{\mathrm{ave}}(R)$ the interaction-induced isotropic dipole polarizability. Equation (1) was used in Refs. 1 and 3 to compute the second dielectric and refractivity virial coefficients of helium and argon.

The general expression for the polarization of an atomic gas placed in an uniform electric field was given by Hill.[31,32] His formula though does not lead to the correct classical limit at high temperatures, due to some simplifications in its derivation. In 1995 Moszynski *et al.* derived a quantum-statistical expression for the second dielectric virial coefficient exhibiting the correct physical behavior, i.e., reducing to the classical result at high temperatures.[25] It is this expression that we briefly present here, leaving the details to the original paper.

Downloaded 26 Jul 2002 to 141.52.232.84. Redistribution subject to AIP license or copyright, see http://ojps.aip.org/jcpo/jcpcr.jsp

The dielectric second virial coefficient can be evaluated as second derivative of the field-dependent ordinary (pressure) second gas virial coefficient $B_2(T;F)$ taken at zero field,

$$B_\epsilon(T)=\frac{4\pi k_B T}{3}\left(\frac{\partial^2 B_2(T;F)}{\partial F^2}\right)_{F=0}, \tag{2}$$

which in turn can be written in terms of the Slater sum, $W(\mathbf{R};F)$:[33]

$$B_2(T;F)=\tfrac{1}{2}\int [W(\mathbf{R};F)-1]d\mathbf{R}, \tag{3}$$

$$W(\mathbf{R};F)=\lambda_B^3\langle \mathbf{R}|e^{-\beta\mathcal{H}(F)}|\mathbf{R}\rangle+\frac{\lambda_B^3(-1)^{2I}}{2I+1}\times\langle -\mathbf{R}|e^{-\beta\mathcal{H}(F)}|\mathbf{R}\rangle. \tag{4}$$

Here $\mathbf{R}$ denotes the coordinate vector, $\langle \mathbf{R}'|X|\mathbf{R}\rangle$ the matrix element of operator X in the coordinate representation, and $\beta=1/k_BT$. I is the nuclear spin quantum number and $\mathcal{H}(F)$ the Hamiltonian of the dimer in the uniform electric field F,

$$\mathcal{H}(F)=-\frac{\hbar^2}{m}\nabla^2+V(R)-\frac{1}{2}\Delta\alpha_{zz}(\mathbf{R})F^2+\mathcal{O}(F^4), \tag{5}$$

where we have introduced the atomic mass m and the zz component of the interaction-induced electric dipole polarizability $\Delta\alpha_{zz}(\mathbf{R})$. The thermal wavelength λ_B is given by $\lambda_B=\sqrt{2\pi\hbar^2/k_BT\mu}$ with the reduced mass $\mu=m/2$.

Taking the derivative with respect to the field, Eq. (2), the second dielectric virial coefficient can be written, after some algebraic manipulations, in terms of $\Delta\alpha_{zz}(\mathbf{R})$ and of the zero-field Slater sum $W(\mathbf{R};0)$:

$$B_\epsilon(T)=\frac{2\pi}{3}\int_0^\infty W(\mathbf{R};0)\Delta\alpha_{zz}(\mathbf{R})d\mathbf{R}. \tag{6}$$

Note that the interaction-induced polarizability can be written in terms of an isotropic—$\Delta\alpha_{\mathrm{ave}}(R)$—and an anisotropic—$\Delta\alpha_{\mathrm{ani}}(R)$—contribution,

$$\Delta\alpha_{zz}(\mathbf{R})=\Delta\alpha_{\mathrm{ave}}(R)+\tfrac{2}{3}\Delta\alpha_{\mathrm{ani}}(R)P_2(\cos\vartheta), \tag{7}$$

with $P_2(\cos\vartheta)$ denoting the second Legendre polynomial and ϑ the angle between the z axis and the dimer axis. The anisotropy disappears from the equations when the integration over ϑ is carried out in Eq. (6). The Slater sum at zero field in Eq. (6) can be evaluated by introducing a complete set of eigenfunctions of $\mathcal{H}_0=\mathcal{H}(0)$:[25]

$$\mathcal{H}_0\Psi_{nJM}=E_{nJ}\Psi_{nJM}, \tag{8}$$

$$\mathcal{H}_0\Psi_{kJM}=\frac{\hbar^2k^2}{2\mu}\Psi_{kJM}=E_k\Psi_{kJM} \tag{9}$$

for the bound—Eq. (8)—and continuum—Eq. (9)—states, respectively, with wave functions

$$\Psi_{nJM}(R)=\frac{1}{R}\chi_{nJ}(R)Y_M^J(\vartheta,\varphi), \tag{10}$$

$$\Psi_{kJM}(R)=\frac{1}{\hbar R}\sqrt{\frac{\mu}{k}}\chi_{kJ}(R)Y_M^J(\vartheta,\varphi). \tag{11}$$

The radial wave functions are solutions of the radial Schrödinger equation

$$-\frac{\hbar^2}{2\mu}\frac{d^2\chi}{dR^2}+\left[V(R)+\frac{\hbar^2J(J+1)}{2\mu R^2}-E\right]\chi=0. \tag{12}$$

Again, after some algebra, the Slater sum can be shown to become[34,35]

$$W(\mathbf{R};0)=\lambda_B^3\sum_{J=0}^\infty\left(1+\frac{(-1)^{J+2I}}{2I+1}\right)\times\left[\sum_{nM}e^{-E_{nJ}/k_BT}\chi_{nJ}^*(R)\chi_{nJ}(R)\times R^{-2}Y_M^{J*}(\vartheta,\varphi)Y_M^J(\vartheta,\varphi)+\int_0^\infty e^{-\hbar^2k^2/2\mu k_BT}\chi_{kJ}^*(R)\chi_{kJ}(R)R^{-2}\times\left(\sum_M Y_M^{J*}(\vartheta,\varphi)Y_M^J(\vartheta,\varphi)\right)dk\right]. \tag{13}$$

In our case the wave functions are normalized as follows:

$$\int_0^\infty\chi_{nJ}^*(R)\chi_{n'J}(R)dR=\delta_{nn'}, \tag{14}$$

$$\int_0^\infty\chi_{kJ}^*(R)\chi_{k'J}(R)dR=\delta(k-k'). \tag{15}$$

Note the different normalization condition employed here for the continuum wave functions with respect to that adopted by Moszynski and co-workers.[25] Using these relationships the dielectric second virial coefficient can be written as

$$B_\epsilon(T)=\frac{2\pi\lambda_B^3}{3}\sum_{J=0}^\infty(2J+1)\left(1+\frac{(-1)^{J+2I}}{2I+1}\right)\times\left(\sum_n e^{-E_{nJ}/k_BT}\langle\chi_{nJ}(R)|\Delta\alpha_{\mathrm{ave}}(R)|\chi_{nJ}(R)\rangle+\int_0^\infty e^{-\hbar^2k^2/2\mu k_BT}\times\langle\chi_{kJ}(R)|\Delta\alpha_{\mathrm{ave}}(R)|\chi_{kJ}(R)\rangle\frac{\mu}{\hbar^2k}dk\right), \tag{16}$$

which involves matrix elements of the interaction-induced average electric dipole polarizability $\Delta\alpha_{\mathrm{ave}}(R)$ over the complete set of bound and continuum wave functions of the zero-field Hamiltonian $\mathcal{H}_0$.

III. COMPUTATIONAL DETAILS

To evaluate the necessary integrals for the quantum-statistical second dielectric virial coefficients Eq. (16) we employed a version of the KORG program[36] originally written by Cacelli, which has been adapted for the present purposes. The interatomic potentials for He_2 and Ar_2 and the interaction-induced polarizabilities for these two van der Waals dimers are taken from Refs. 2 and 37.

Downloaded 26 Jul 2002 to 141.52.232.84. Redistribution subject to AIP license or copyright, see http://ojps.aip.org/jcpo/jcpcr.jsp

TABLE I. Parameters of the least-squares fits of the extrapolated FCI/d-aug-cc-pV5Z-3321 He_2 (see the text) and the CCSD(T)/d-aug-cc-pV5Z-33211 Ar_2 (Ref. 37) potentials to HFD-B like functional forms (Ref. 40), Eqs. (17) and (24). The numerical values of the parameters are given for the internuclear distance R in a.u. and the potential energy in K.

Parameter	Helium	Argon	Dimension
A^*	186 924.404	132 354.926	⋯
α^*	9.872 630 46	8.150 337 34	⋯
β^*	−1.721 587 17	−1.609 293 46	⋯
c_6	2.114 098 95	3.076 264 23	⋯
c_8	0.671 454 04	1.940 602 74	⋯
c_{10}	0.283 390 47	3.169 037 01	⋯
r_m	2.783 100 09	3.169 396 36	Å
D	1.438 0		⋯
ϵ/k_B	10.412 321 71	143.235	K
ρ		1.107	⋯

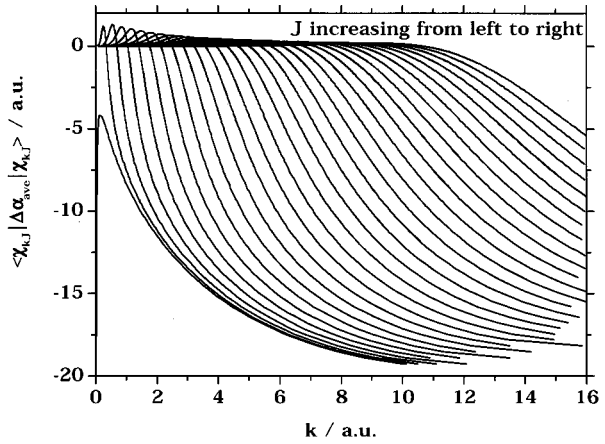


FIG. 1. He_2. The matrix element $\langle \chi_{kJ}|\Delta\alpha_{\rm ave}|\chi_{kJ}\rangle$ as function of the momentum k for $J=0,2,4,...,60$ (in a.u.).

A. Helium

In our previous study[3] we found that as the temperature decreases the virial coefficients obtained in the semiclassical approximation become particularly sensitive to the potential in the region around the equilibrium distance and to the description of the repulsive wall. We have therefore determined a new very accurate *ab initio* potential for He_2 by correcting the FCI/d-aug-cc-pVTZ-3321 interaction potential from Ref. 2 for remaining basis set effects with the difference between the CCSD(T)/d-aug-cc-pVTZ-3321 and the CCSD(T)/d-aug-cc-pV5Z-3321 results. The resulting potential—in the following referred to as ''extrapolated FCI/d-aug-cc-pV5Z-3321''—is expected to be the most accurate He_2 potential available for such a large range of internuclear distances (3.0–13.0 a.u.), in particular in the region of the repulsive wall. The numerical values are available for 25 internuclear distances.[38] To obtain an accurate interpolation between these points and a reliable extrapolation below 3.0 a.u. and beyond 13.0 a.u., we fitted to the *ab initio* calculated points a HFD-B like analytic potential function:[39]

$$V(R)=\frac{\epsilon}{k_B}V^*(Ra_0/r_m), \tag{17}$$

$$V^*(r)=A^*e^{-\alpha^* r+\beta^* r^2}-F(r)\sum_{n=0}^{2}\frac{c_{6+2n}}{r^{6+2n}}, \tag{18}$$

$$F(r)=\begin{cases}\exp(-(D/r-1)^2) & \text{for} \quad r\leqslant D\\ 1 & \text{for} \quad r\geqslant D\end{cases}. \tag{19}$$

The parameters ϵ/k_B, α^*, β^*, r_m, c_6, c_8, and c_{10} were determined by a least-squares fit; the multiplicative constant A^* and the parameter D were taken from Ref. 39. The numerical values for the parameters are listed in Table I.

For the interaction-induced polarizability we used the extrapolated FCI/d-aug-cc-pV5Z-3321 results from Ref. 2. They were obtained after correcting for remaining basis set effects the FCI/d-aug-cc-pVTZ-3321 results for $\Delta\alpha_{\rm ave}(R)$ with the differences between the CCSD/d-aug-cc-pV5Z-3321 and the CCSD/d-aug-cc-pVTZ-3321 results. For $\Delta\alpha_{\rm ave}(R)$ the *ab initio* calculated points were fitted to the function

$$\Delta\alpha_{\rm ave}(R)=-D\exp[-(R-\sigma)^2/\rho]+A_6R^{-6}, \tag{20}$$

where the parameters (in atomic units) were determined by a least-squares fit as[2] $\sigma=-2.5288$, $D=8.3152$, $\rho=8.1515$, and $A_6=47.094$. These analytic functions were then directly used in the KORG program to evaluate the internuclear potential and $\Delta\alpha_{\rm ave}(R)$ at the grid points for the numerical integrations in the internuclear distance R. The latter were carried out using an even spaced grid between 0.5 and 100.0 a.u. with an increment of 0.001 a.u., i.e., 99501 grid points. The ^{4}He atomic mass was taken as 4.002 603 24 u.

As shown in Fig. 1, for helium the matrix elements $\langle \chi_{kJ}|\Delta\alpha_{\rm ave}(R)|\chi_{kJ}\rangle$ are smooth and slowly varying functions of the momentum k. The numerical integration over k can therefore be carried out accurately by a trapezoidal rule quadrature with even spaced points. We used a grid between 0.01 and 16.0 a.u. with a step length of 0.001 a.u., i.e., 15 991 points. The summation over the angular moment J was found to converge relatively fast: at $J=60$ the second dielectric virial coefficient B_ϵ is converged within $\pm 1\%$ and at $J=70$, which was used as upper limit in the present calculations, convergence within $\pm 0.1\%$ is expected.

In order to investigate the quantum effect on the dispersion in the frequency-dependent case, i.e., for the second refractivity virial coefficient, we expand the frequency-dependent interaction-induced polarizability and the refractive index as

$$\Delta\alpha_{\rm ave}(R,\omega)=\Delta\alpha_{\rm ave}(R)+\omega^2\Delta S_{\rm ave}(-4)(R)+\mathcal{O}(\omega^4), \tag{21}$$

$$B_R(T,\omega)=B_\epsilon(T)+\omega^2B_R^{(2)}(T)+\mathcal{O}(\omega^4), \tag{22}$$

where $\Delta S_{\rm ave}(-4)(R)$ is the isotropic average of the interaction-induced Cauchy moment of order -4. To evaluate the dispersion coefficient $B_R^{(2)}(T)$ we applied the same procedure as described previously for $B_\epsilon(T)$, but with $\Delta S_{\rm ave}(-4)(R)$ as interaction-induced property instead of $\Delta\alpha_{\rm ave}(R)$. For $\Delta S_{\rm ave}(-4)(R)$ the ''extrapolated FCI/d-aug-cc-pV5Z-3321'' results from Ref. 2 were employed, which have been fitted to the same expression as used for the static interaction-induced isotropic polarizability, given in Eq. (20).

Downloaded 26 Jul 2002 to 141.52.232.84. Redistribution subject to AIP license or copyright, see http://ojps.aip.org/jcpo/jcpcr.jsp

For $\Delta S_{\mathrm{ave}}(-4)(R)$ the values of the parameters are: $\sigma = -1.0570$, $D=4.6597$, $\rho=7.2720$, and $A_6=110.136$. The quantum statistical calculations for the dispersion coefficient $B_R^{(2)}(T)$ were carried out using the same integration ranges and grids as used for the (static) second dielectric virial coefficients.

B. Argon

The van der Waals potential for the argon dimer has a deep well which supports up to nine bound vibrational states depending on the angular momentum J. In contrast to He_2, for $J>0$ the effective potential in the vibrational Schrödinger equation is not purely repulsive, but it has a well and a finite barrier before it goes asymptotically to zero as $J(J+1)/R^2$. As a consequence of this the vibrational spectrum of Ar_2 contains, in addition to bound and purely continuum states, also quasibound states (resonances) which make the numerical integration over the momentum k in Eq. (16) a difficult task. These quasibound states are found at approximately those energies for which a model potential in which the finite barrier has been substituted by an infinitely thick wall has additional bound states. Unlike bound states, the quasibound states have a finite lifetime and width (in E or k), which can vary by several orders of magnitude depending on the energy and the barrier width. While for purely continuum states with energies below the barrier height the amplitude of the wave function is very small inside the barrier, for quasibound states the amplitudes are largest inside the barrier and almost negligible outside. We define the function

$$A(k)=\int_0^{R_{\max}} \frac{\mu}{\hbar^2 k}\chi_{kJ}^*(R)\chi_{kJ}(R)dR \tag{23}$$

as the measure of the probability density inside in the barrier as a function of k. $R_{\max}$ is the internuclear distance where the maximum height of the potential curve occurs. $A(k)$ is small for true continuum states, but it becomes large for quasibound states and the integral of $A(k)$ over the width of the state is in the order of 1, i.e., quasibound states give similar large contributions to the virial coefficients as true bound states. Figure 2 shows the behavior of the $A(k)$ function for the argon dimer for $J=48$. It represents the typical situation: for the lowest quasibound state at $k\approx 3.8$ a.u. $A(k)$ has a very narrow and rather high peak, while for the quasibound states located higher in energy the peaks become broad and less pronounced. As shown in Fig. 3, this behavior is reflected in the matrix elements of the interaction-induced polarizability $\langle \chi_{kJ}|\Delta\alpha_{\mathrm{ave}}(R)|\chi_{kJ}\rangle$. It is thus impossible to evaluate the integral over the momentum k efficiently and accurately using a fixed step length. Therefore, we have implemented a numerical integration scheme which locates the position of the quasibound states and automatically adapts its step lengths around this position. The procedure can be summarized in the following points.

(1) For each value of J the occurrence of maxima in the effective potential $V(R)+[\hbar^2 J(J+1)]/2\mu R^2$ is verified and, if the maximum is found, the energies of the quasibound states are determined by locating the maxima of $A(k)$.

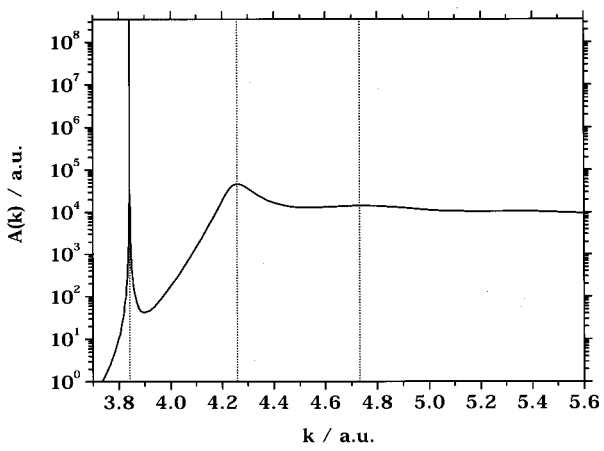


FIG. 2. Ar_2. The integral $A(k)$ [Eq. (23)] for $J=48$ (in a.u.). The vertical lines indicate the positions of the three lowest resonances.

(2) The matrix elements for $\Delta\alpha_{\mathrm{ave}}(R)$ are calculated at the boundaries for k, i.e., the lower and upper integration limits, at the positions of the quasibound states, and at one additional point between each of these positions.

(3) The actual set of points is interpolated (in k) by a cubic spline function and a comparison is made with a linear interpolation.

(4) If the integrated mean square difference between the cubic and the linear interpolation is above a given threshold, additional points are inserted in those intervals in which the largest differences occur.

(5) The scheme continues at step (3) until the integrated mean square difference between the two curves is below the threshold.

This procedure allows an accurate and efficient integration of the matrix elements over k independent of the height and width of the peaks caused by quasibound states. For Ar_2, a convergence in the integral of the $\Delta\alpha_{\mathrm{ave}}(R)$ matrix element over k within 0.05% was usually obtained with 300–3000 points (in k), depending on the number of quasibound states and their width. The interval used for the integration over the momentum was $k=0.5$–150 a.u.

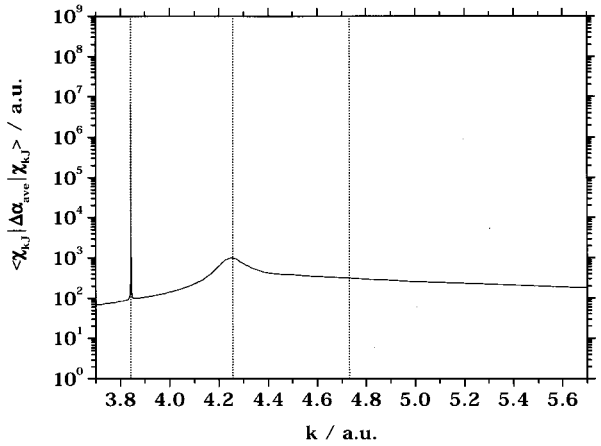


FIG. 3. Ar_2. The matrix element $\langle \chi_{kJ}|\Delta\alpha_{\mathrm{ave}}|\chi_{kJ}\rangle$ as a function of the momentum k for $J=48$ (in a.u.). The vertical lines indicate the positions of the three lowest resonances.

Downloaded 26 Jul 2002 to 141.52.232.84. Redistribution subject to AIP license or copyright, see http://ojps.aip.org/jcpo/jcpcr.jsp

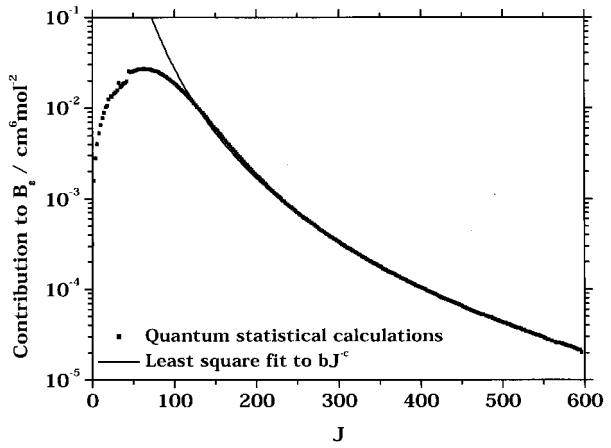


FIG. 4. Argon. Convergence of the contributions to $B_\epsilon(T)$ with J. Quantum statistical results and results of the least-squares fit to the function bJ^{-C}.

Another problem emerging for Ar_2 and which was not perceptible for the much more weakly bound He_2 complex, is the slow convergence of the sum over the angular momentum J in Eq. (16). In the range of temperatures studied here the value of the virial coefficient $B_\epsilon(T)$ is not converged (within 0.1%) even for J as high as 400. However, as shown in Fig. 4, for large angular momenta the contributions to $B_\epsilon(T)$ are found to decrease approximately as $b \cdot J^{-C}$, where b and C depend on the temperature. For a given maximum angular momentum $J_{\max}$ this extrapolation can be used to estimate the remaining contributions for $J > J_{\max}$ and thereby to improve and test the convergence of $B_\epsilon(t)$. The parameters b and C can be calculated from the original results for $J_{\max}$ and $J_{\max}-2$. The final results reported in Sec. IV were obtained employing this extrapolation with $J_{\max}=600$. For this value the size of the extrapolated correction was decreased below 0.3% for all investigated temperatures and the extrapolated results were converged within 0.01%.

For the calculations on argon we employed the CCSD(T)/d-aug-cc-pV5Z-33211 potential from Ref. 37. This potential is available for a total of 59 internuclear distances in the range between 3.8 and 20.0 a.u. To obtain an accurate interpolation between these points and a reliable extrapolation beyond 20.0 a.u., we fitted the CCSD(T)/d-aug-cc-pV5Z-33211 points to a HFD-B like functional form with a doubly corrected dispersion series:[40]

$$V(R) = \frac{\epsilon}{k_B} V^*(R), \tag{24}$$

$$V^*(R) = A^* \exp\left(-\alpha^* \frac{Ra_0}{r_m} + \beta^* \left(\frac{Ra_0}{r_m} \right)^2 \right) - f(\rho R) \sum_{n=0}^{2} \frac{c_{6+2n}}{\left(Ra_0/r_m \right)^{6+2n}} g_{6+2n}(\rho R), \tag{25}$$

$$g_n(x) = (1 - \exp(-2.1x/n - 0.109x^2/\sqrt{n}))^n, \tag{26}$$

$$f(x) = 1 - x^{1.68} e^{-0.78x}. \tag{27}$$

The parameters A^*, α^*, β^*, r_m, c_6, c_8, and c_{10} were determined by a least-squares fit, while the values for ϵ/k_B and ρ where taken from Ref. 40 and a_0 is the Bohr radius. The numerical values of the parameters are given in Table I. For the interaction-induced polarizability we used the CCSD/d-aug-cc-pVQZ-33211 results from Ref. 2. These are available for 12 distances between 5.5 and 30.0 a.u. To interpolate between these points and to extrapolate beyond them we employed the fit to the functional form

$$\Delta\alpha_{\text{ave}}(R) = -\exp(-(R-\sigma)/\rho) + \sum_{n=0}^{3} A_{6+2n} R^{-6-2n} \tag{28}$$

given in Ref. 2. The parameters are (a.u.): $\sigma=6.1589$, $\rho=0.7028$, $A_6=8876.3$, $A_8=-450\,859$, $A_{10}=1.2318\times10^8$, and $A_{12}=-1.7660\times10^9$. From these analytical functions the interaction potential and the interaction-induced polarizability were evaluated on a total of 341 points as input to KORG, which then employed a cubic spline interpolation between these points to evaluate the potential and $\Delta\alpha_{\text{ave}}(R)$ at the grid points for the numerical integrations in R, needed for the solution of the vibrational Schrödinger equation and the calculation of the matrix elements for $\Delta\alpha_{\text{ave}}(R)$. The latter were carried out on an even spaced grid for R between 0.5 and 300 a.u. with an increment of 0.0005 a.u. The argon atomic mass was taken as 39.9623 837 u.

For argon we have not evaluated the quantum effect on the dispersion of the refractive index since from Ref. 3 it is known that for argon the dispersion contributes for $\lambda > 500$ nm only with a few percent to $B_R(T,\omega)$. The small quantum effect on this small contribution will thus clearly be negligible for a comparison between theoretical and experimental results, with the accuracies that can be reached nowadays.

IV. RESULTS AND DISCUSSION

A. Helium

The results for the second dielectric virial coefficient $B_\epsilon(T)$ of helium are presented in Table II and in Fig. 5. A comparison is made with the semiclassical results from our previous study,[3] the quantum statistical results from Moszynski *et al.*,[25] and the available experimental data.

Let us first compare the present quantum statistical calculation with those of the results of the previous semiclassical study.[3] As known from the work of Moszynski *et al.*,[25] for higher temperatures the results obtained with the two approaches converge fast to the same values. Above $T=70$ K the differences are practically insignificant considering the accuracy of the *ab initio* calculations. One also has to bear in mind that the two calculations were carried out with different potentials, although the effect of using different potentials is probably small at these temperatures. At low temperatures the differences between the semiclassical and the quantum statistical approaches become perceptible and below $T=7$ K the semiclassical results start a steep decrease whereas the curvature of the quantum statistical results remains almost constant.

Comparing the present results for $B_\epsilon(T)$ with those of the previous quantum statistical calculation obtained by Moszynski *et al.*,[25] one observes that both curves show the same qualitative behavior. The present results are basically

Downloaded 26 Jul 2002 to 141.52.232.84. Redistribution subject to AIP license or copyright, see http://ojps.aip.org/jcpo/jcpcr.jsp

TABLE II. Helium. Temperature dependence of the second dielectric virial coefficient $B_\epsilon(T)$. Compared are the semiclassical (SC) values from Ref. 3, the quantum-statistical (QS) results from this work, the quantum-statistical results from Ref. 25, and the available experimental values. For computational details of the present calculations see Sec. III. The dispersion contribution is given in terms of $B_R^{(2)}(T)$ ($B_R(T)=B_\epsilon(T)+\omega^2 B_R^{(2)}(T)$). The units are for the temperature K and for the virial coefficients $B_\epsilon(T)$ and $B_R^{(2)}(T)$ $\mathrm{cm}^6\,\mathrm{mol}^{-2}$ where the frequency ω in the above equation is assumed to be given in a.u.

T	$B_\epsilon(T)$ SC Ref. 3	$B_\epsilon(T)$ QS This work	$B_R^{(2)}(T)$ SC Ref. 3	$B_R^{(2)}(T)$ QS This work	$B_\epsilon(T)$ QS Ref. 25	$B_\epsilon(T)$ Experiment	Ref.
3.799	−0.0731	−0.0016	−0.6271	−0.0709	−0.0081	−0.023[a]	19
4.220	−0.0549	−0.0017	−0.4840	−0.0696	−0.0081	−0.083±0.026	15
7.199	−0.0187	−0.0025	−0.1892	−0.0676	−0.0092	−0.036±0.026	15
13.804	−0.0106	−0.0047	−0.1112	−0.0731	−0.0104	−0.010±0.026	15
20.271	−0.0105	−0.0068	−0.1006	−0.0804	−0.0123	−0.062±0.010	15
27.098	−0.0116	−0.0089	−0.1001	−0.0880	−0.0144	−0.088±0.026	15
77.400	−0.0220	−0.0210	−0.1324	−0.1335	−0.0265	−0.02±0.02	7
100.00	−0.0262	−0.0254	−0.1471	−0.1497	−0.0309		
130.00	−0.0313	−0.0307	−0.1651	−0.1687			
160.00	−0.0361	−0.0354	−0.1814	−0.1856			
180.00	−0.0390	−0.0384	−0.1916	−0.1960			
200.00	−0.0419	−0.0412	−0.2012	−0.2058	−0.0466		
220.00	−0.0446	−0.0439	−0.2104	−0.2151			
242.95	−0.0475	−0.0469	−0.2203	−0.2252	−0.0522	−0.07±0.01	7
253.00	−0.0488	−0.0482	−0.2245	−0.2294			
261.00	−0.0497	−0.0491	−0.2278	−0.2328			
274.00	−0.0513	−0.0507	−0.2330	−0.2380			
287.00	−0.0528	−0.0522	−0.2380	−0.2432			
293.00	−0.0535	−0.0529	−0.2403	−0.2455			
296.00	−0.0538[b]	−0.0533	−0.2415	−0.2466			
298.15	−0.0541	−0.0535	−0.2423	−0.2475	−0.0587	−0.11±0.02	6
						−0.08±0.01	16
303.00	−0.0546	−0.0541	−0.2441	−0.2493	−0.0592	−0.059±0.009	17
						−0.06±0.01	18
315.00	−0.0560	−0.0554	−0.2485	−0.2538			
322.15	−0.0567	−0.0562	−0.2511	−0.2564	−0.0613	−0.06±0.04	11
323.00	−0.0568	−0.0563	−0.2514	−0.2567	−0.0614	−0.068±0.01	14
323.15	−0.0569	−0.0563	−0.2514	−0.2568	−0.0614	−0.07±0.01	7
340.00	−0.0587	−0.0582	−0.2573	−0.2628			
375.00	−0.0622	−0.0618	−0.2691	−0.2748			
407.60	−0.0654	−0.0651	−0.2794	−0.2855			

[a]Also −0.030±0.004, Ref. 19 for ^{3}He at 4 K.
[b]Compared with −0.0614, calculated at MP4 level by Bishop and Dupuis (Ref. 42).

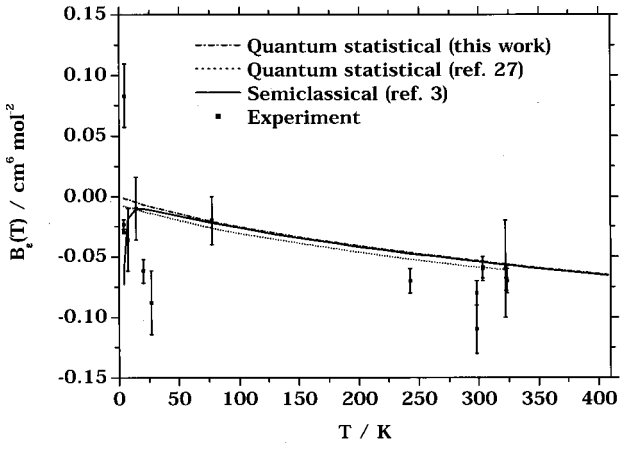


FIG. 5. Helium. Temperature dependence of the second dielectric virial coefficient $B_\epsilon(T)$. Semiclassical (Ref. 3), quantum-statistical (this work and Ref. 25), and experimental results in comparison.

shifted by about 0.005 $\mathrm{cm}^6\,\mathrm{mol}^{-2}$ compared to the results from Ref. 25. At very small temperatures ($T<30$ K), where $B_\epsilon(T)$ becomes small, this gives rise to rather large relative differences (a factor between 1.5 and 4). The origin of this disagreement is most likely the use of different input data, in particular for the interaction-induced polarizability. For their quantum statistical calculations Moszynski and co-workers used the empirical He_2 potential determined by Aziz *et al.*[41] and the interaction-induced polarizability from a SAPT calculation[26] in a $[5s4p3d2f]$ basis set. The error of the interaction-induced polarizability from the SAPT calculation was estimated to be of ≈5%. The extrapolated FCI/d-aug-cc-pV5Z-3321 interatomic potential and interaction-induced polarizability are expected to be more accurate than the empirical potential from Ref. 41 and the SAPT interaction-induced polarizabilities since, due to the basis set extrapolation, the results of the FCI calculations should be close to the

Downloaded 26 Jul 2002 to 141.52.232.84. Redistribution subject to AIP license or copyright, see http://ojps.aip.org/jcpo/jcpcr.jsp

basis set limit. From the small differences between our present results and those of the semiclassical calculations presented in Ref. 3, which were obtained with the same empirical potential used by Moszynski *et al.* but employing the FCI interaction-induced polarizability, we conclude that the effect of the small differences in the potential curve is after all small and that most of the differences between the present results and those from Ref. 25 can be attributed to the improved interaction-induced polarizabilities.

As shown in Fig. 5, the available experimental data carry rather large error bars and do not agree well with either of the two quantum statistical calculations. Thus, no conclusions about the accuracy of the theoretical calculations can be drawn from a comparison with experiment. The large discrepancies between the theoretical and the experimental results and also between the experimental results from different measurements call, however, for new experimental determinations of the second dielectric virial coefficient of helium.

Regarding the frequency dependence of the second refractivity virial coefficient $B_R(T,\omega)$, we find that the quantum effects on the dispersion of $B_R(T,\omega)$ follow the same pattern as for the static contribution: at very low temperatures a quantum statistical approach is even essential to obtain qualitatively correct results, but with increasing temperature the quantum effects decrease and are (almost) insignificant for temperatures larger 77 K.

For helium gas the quantum effects increase the relative dispersion of the second refractivity virial coefficient defined by $B_R^{(2)}(T,\omega)/B_\epsilon(T)$. For example, at 4.22 K and 632.8 nm, dispersion accounts for about 19% of B_R. With increasing temperature the dispersion contribution becomes smaller as the quantum effect diminishes.

B. Argon

Table III and Fig. 6 show the quantum statistical results for the second dielectric virial coefficient of argon and a comparison with the semiclassical calculation of Ref. 3 and with the available experimental data. The atomic mass of argon is about an order of magnitude larger than that of helium, and the thermal wavelength is thus about a factor of 3 shorter. One could thus expect quantum effects to be less important for argon than for helium. On the other hand, the argon dimer potential has a much deeper well supporting several bound and quasibound states which could lead to pronounced quantum effects at lower temperatures. However, as seen in Table III and Fig. 6 we find that in the experimentally investigated range of temperatures between 243 and 408 K quantum effects are negligible. They are $\approx 0.5\%-1.0\%$, which is close to the accuracy of the interpolations and the numerical integrations carried out in the calculation of $B_\epsilon(T)$. This effect is also below the accuracy of the interaction-induced polarizabilities used, which were obtained from CCSD calculations with the d-aug-cc-pVQZ-33211 basis set. From a comparison of the semiclassical results obtained with the CCSD/d-aug-cc-pVQZ-33211 polarizability with those obtained using the CCSD/d-aug-cc-pVTZ-33211 data[3] we estimate that the remaining basis set effects on $B_\epsilon(T)$ will be on the order of a few percent. As the temperature decreases, as expected, the difference between semiclassical and quantum statistical results increase. The quantum statistical estimate at 100 K is about 3% lower than the corresponding semiclassical value. To our knowledge though no experimental data are available for B_ϵ of argon at temperatures lower than 243 K.

Thus quantum effects do not alter the comparison with experimental data from Refs. 1 and 3 and the conclusions drawn thereof. The uncertainties of the experimental determinations are much larger than those of the *ab initio* calculations—including remaining correlation and basis set effects and the numerical errors in the calculation of the virial coefficients. Since also the agreement between experi-

TABLE III. Argon. The second virial coefficient $B_\epsilon(T)$ computed at the semiclassical and the quantum statistical level. The temperature T is given in K, and the virial coefficients $B_\epsilon(T)$ in $\mathrm{cm}^6\,\mathrm{mol}^{-2}$.

	$B_\epsilon(T)$		
T	Semiclassical	Quantum statistical	Experiment
100.00	2.23	2.16	
120.00	1.99	1.94	
140.00	1.84	1.80	
160.00	1.74	1.70	
180.00	1.66	1.63	
200.00	1.59	1.57	
220.00	1.54	1.52	
242.95	1.49	1.48	1.84 ± 0.07[a]
253.00	1.47	1.46	
261.00	1.46	1.45	
274.00	1.44	1.42	
287.00	1.42	1.41	
296.00	1.41	1.39	2.52(34),[b] 1.73(34),[b] 1.81(34)[b]
298.15	1.40	1.39	0.79 ± 0.10,[c] 1.57 ± 0.58,[d] 2.16 ± 0.34,[e] 1.49 ± 0.15[f]
300.00	1.40[g]	1.39	
303.15	1.40	1.38	1.22 ± 0.09,[a] 1.23 ± 0.05,[h] 1.75 ± 0.05[i]
306.15	1.39	1.38	1.0 ± 2.1[j]
315.00	1.38	1.37	
322.00	1.37	1.36	0.726,[k] 0.39 ± 0.20[l]
323.00	1.37	1.36	0.72 ± 0.13,[m] 1.76 ± 0.05[n]
340.00	1.35	1.34	
370.00	1.31	1.31	
407.60	1.28	1.27	0.1 ± 0.3[a]

[a]Reference 7.
[b]Reference 43; second refractivity virial coefficient at 296.82 K: 2.52(34) $\mathrm{cm}^6\,\mathrm{mol}^{-2}$ at 594.096 nm, 1.73(34) $\mathrm{cm}^6\,\mathrm{mol}^{-2}$ at 543.516 nm, 1.81(34) $\mathrm{cm}^6\,\mathrm{mol}^{-2}$ at 325.530 nm.
[c]Reference 6.
[d]Reference 44; second refractivity virial coefficient at 296.2 K: 1.57 ± 0.58 $\mathrm{cm}^6\,\mathrm{mol}^{-2}$ at 632.8 nm, 1.55 ± 0.74 $\mathrm{cm}^6\,\mathrm{mol}^{-2}$ at 514.5 nm, 1.58 ± 0.69 $\mathrm{cm}^6\,\mathrm{mol}^{-2}$ at 488.0 nm, 1.53 ± 0.32 $\mathrm{cm}^6\,\mathrm{mol}^{-2}$ at 457.9 nm.
[e]Reference 45; second refractivity virial coefficient at 296.2 K and 632.99 nm.
[f]Reference 46; second refractivity virial coefficient at 296.2 K and 632.99 nm.
[g]From a DID model: 1.53 $\mathrm{cm}^6\,\mathrm{mol}^{-2}$, Ref. 47.
[h]Reference 8.
[i]Reference 18; second refractivity virial coefficient at 632.99 nm.
[j]Reference 10.
[k]From CIS measurements, Ref. 12.
[l]Reference 11.
[m]Reference 9.
[n]Reference 14; second refractivity virial coefficient at 632.99 nm.

Downloaded 26 Jul 2002 to 141.52.232.84. Redistribution subject to AIP license or copyright, see http://ojps.aip.org/jcpo/jcpcr.jsp

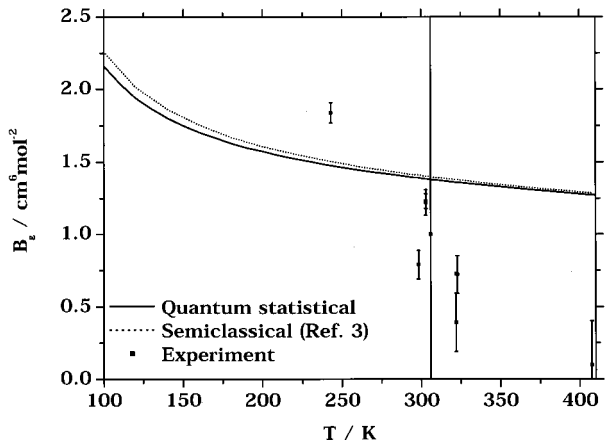


FIG. 6. Argon. Temperature dependence of the second dielectric virial coefficient $B_\epsilon(T)$, semiclassical results of Ref. 3, and experimental values.

mental results from different measurements is only limited, an experimental reexamination of the second dielectric virial coefficient of argon would be warranted.

In the present investigation for argon we have not considered the frequency-dependent case, i.e., the second refractivity virial coefficient. This has been done in detail in previous work[1,3] where we calculated the first nonvanishing dispersion coefficient $B_R^{(2)}(T)$ within a semiclassical framework. For the experimentally investigated range of frequencies the difference between $B_R(T,\omega)$ and $B_\epsilon(T)$ was, however, found to be relatively small compared to the discrepancy between *ab initio* calculated and experimental results. Since for argon the quantum effect on $B_\epsilon(T)$ is apparently very small, the cross term coming from the quantum effect on the small dispersion contribution to $B_R(T)$ will be insignificant compared to other error sources, as, e.g., missing higher-order correlation contributions or incompleteness of the one-electron basis set.

V. CONCLUSIONS

We extended our previous studies of the second dielectric virial coefficients of He_2 and Ar_2, which were based on a semiclassical approximation, to a fully quantum statistical approach. For helium our results support the findings of Moszynski *et al.*,[25] namely that quantum effects become substantial below 10–7 K and that most of the experimental results for low temperatures are in significant disagreement with theory. Since also the scattering of data from different measurements is rather large for $T<70$ K, the experimental results in this temperature range need to be reconsidered.

For argon, we find that at least in the investigated range of temperatures (100–408 K) quantum effects are negligible compared to the accuracy that can be obtained for $B_\epsilon(T)$. The quantum statistical results are at most $\approx 3\%$ lower than the corresponding semiclassical counterparts at the lower end of the temperature interval. Differences drop to less than 1.1% above 240 K, where all the available experimental data lie. The semiclassical approximation is thus justified for Ar_2 above 240 K, and it can be expected to be also valid in this temperature range for gases with similar or larger molecular mass, provided that the van der Waals attraction is of comparable magnitude. Also, for argon a number of experimental results are in disagreement with the *ab initio* calculations, while some other measurements are in reasonable good agreement with the theoretical results. An experimental reinvestigation of the second dielectric virial coefficient of argon would thus be helpful for assessing the accuracy of both *ab initio* calculations and experimental measurements.

ACKNOWLEDGMENTS

We are greatly indebted to Ivo Cacelli for providing the original version of KORG and for fruitful discussions. This work has been supported by the European Research and Training Network ''Molecular Properties and Molecular Materials'' (MOLPROP), Contract No. HPRN-CT-2000-00013, and by the Spanish Comisión Interministerial de Ciencia y Tecnología (PB98-0609-C04-01).

[1] B. Fernández, C. Hättig, H. Koch, and A. Rizzo, J. Chem. Phys. **110**, 2872 (1999).
[2] C. Hättig, H. Larsen, J. Olsen, P. Jørgensen, H. Koch, B. Fernández, and A. Rizzo, J. Chem. Phys. **111**, 10099 (1999).
[3] H. Koch, C. Hättig, H. Larsen, J. Olsen, P. Jørgensen, B. Fernández, and A. Rizzo, J. Chem. Phys. **111**, 10108 (1999).
[4] M. Pecul and A. Rizzo, Mol. Phys. **100**, 447 (2002).
[5] A. Rizzo, K. Ruud, and D. M. Bishop, Mol. Phys. **100**, 799 (2002).
[6] D. Vidal and M. Lallemand, J. Chem. Phys. **64**, 4293 (1976).
[7] J. Huot and T. K. Bose, J. Chem. Phys. **95**, 2683 (1991).
[8] T. K. Bose, K. Boudjarane, J. Huot, and J. M. St-Arnaud, J. Chem. Phys. **89**, 7435 (1988).
[9] T. K. Bose and R. H. Cole, J. Chem. Phys. **52**, 140 (1970).
[10] D. R. Johnston, G. J. Oudermans, and R. H. Cole, J. Chem. Phys. **33**, 1310 (1960).
[11] R. H. Orcutt and R. H. Cole, J. Chem. Phys. **46**, 697 (1967).
[12] M. H. Proffitt, J. W. Keto, and L. Frommhold, Can. J. Phys. **59**, 1459 (1981).
[13] C. G. Joslin, J. D. Goddard, and S. Goldman, Mol. Phys. **89**, 791 (1996).
[14] H. J. Achtermann, G. Magnus, and T. Bose, J. Chem. Phys. **94**, 5669 (1991).
[15] D. Gugan and G. W. Michel, Metrologia **16**, 149 (1980).
[16] M. Lallemand and D. Vidal, J. Chem. Phys. **66**, 4776 (1977).
[17] S. Kirouac and T. K. Bose, J. Chem. Phys. **64**, 1580 (1976).
[18] H. J. Achtermann, J. G. Hong, G. Magnus, R. A. Aziz, and M. J. Slaman, J. Chem. Phys. **98**, 2308 (1993).
[19] E. C. Kerr and R. H. Shermann, J. Low Temp. Phys. **3**, 451 (1970).
[20] A. Ishihara and R. V. Hanks, J. Chem. Phys. **36**, 433 (1962).
[21] A. Ishihara, J. Chem. Phys. **38**, 2437 (1963).
[22] D. A. McQuarrie and H. B. Levine, Physica (Amsterdam) **31**, 749 (1965).
[23] J. F. Ely and D. A. McQuarrie, J. Chem. Phys. **54**, 2885 (1971).
[24] L. W. Bruch, P. J. Fortune, and D. H. Berman, J. Chem. Phys. **61**, 2626 (1974).
[25] R. Moszynski, T. G. A. Heijmen, and A. van der Avoird, Chem. Phys. Lett. **247**, 440 (1995).
[26] R. Moszynski, T. G. A. Heijmen, P. E. S. Wormer, and A. van der Avoird, J. Chem. Phys. **104**, 6997 (1996).
[27] R. Moszynski, Habilitation thesis, University of Warsaw, 1997.
[28] E. A. Mason and T. H. Spurling, *The Virial Equation of State*, The International Encyclopedia of Physical Chemistry and Chemical Physics Vol. 2 Topic 10 (Pergamon, London, 1969).
[29] J. O. Hirschfelder and C. F. Curtiss, *Molecular Theory of Gases and Liquids* (Wiley, New York, 1954).
[30] A. D. Buckingham and J. A. Pople, Discuss. Farady Soc. **22**, 17 (1956).
[31] T. L. Hill, J. Chem. Phys. **28**, 61 (1958).
[32] A. D. Buckingham and R. E. Raab, Trans. Faraday Soc. **54**, 623 (1958).
[33] J. de Boer, Rep. Prog. Phys. **12**, 305 (1949).
[34] J. M. Blatt, Nuovo Cimento **IV**, 430 (1962).
[35] J. M. Blatt, Nuovo Cimento **IV**, 465 (1962).
[36] I. Cacelli, A. Rizzo, and C. Hättig, KORG, a program for the solution of the radial Schrödinger equation for bound and discrete levels.

Downloaded 26 Jul 2002 to 141.52.232.84. Redistribution subject to AIP license or copyright, see http://ojps.aip.org/jcpo/jcpcr.jsp

[37] B. Fernández and H. Koch, J. Chem. Phys. **109**, 10255 (1998).
[38] See EPAPS Document No. E-JCPSA6-117-317230 for the original points of the He_2 potentials. This document may be retrieved via the EPAPS homepage (http://www.aip.org/pubservs/epaps.html) or from ftp.aip.org in the directory /epaps/. See the EPAPS homepage for more information.
[39] R. A. Aziz, A. R. Janzen, and M. R. Moldover, Phys. Rev. Lett. **74**, 1586 (1995).
[40] R. A. Aziz, J. Chem. Phys. **99**, 4518 (1993).
[41] R. A. Aziz, F. R. W. McCourt, and C. C. K. Wong, Mol. Phys. **61**, 1487 (1987).
[42] D. M. Bishop and M. Dupuis, Mol. Phys. **88**, 887 (1996).
[43] U. Hohm, Mol. Phys. **81**, 157 (1994).
[44] R. C. Burns, C. Graham, and A. R. M. Weller, Mol. Phys. **59**, 41 (1986).
[45] A. D. Buckingham and C. Graham, Proc. R. Soc. London, Ser. A **336**, 275 (1974).
[46] R. Coulon, G. Montixi, and R. Occelli, Can. J. Phys. **59**, 1555 (1981).
[47] U. Holm, Z. Naturforsch., A: Phys. Sci. **48a**, 505 (1993).

Downloaded 26 Jul 2002 to 141.52.232.84. Redistribution subject to AIP license or copyright, see http://ojps.aip.org/jcpo/jcpcr.jsp